Role of stratiform rainfall in modifying the northward propagation of monsoon intraseasonal oscillation

R. Chattopadhyay,[1] B. N. Goswami,[1] A. K. Sahai,[1] and K. Fraedrich[2]

[1] The stratiform and convective rain rate measurement from the Tropical Rainfall Measuring Mission (TRMM) satellite data can give a realistic idea of the latent heating distribution in the tropics. The vertical profile of diabatic heating related to the convective and the stratiform rain is known to modulate the dynamical response of atmosphere and also the vertical structure of Madden-Julian Oscillation. In this study, the contribution of the stratiform and convective rain rate to the total rain rate during different phases of the northward propagating boreal summer monsoon intraseasonal oscillation (ISO) is examined using the TRMM data. Two new insights have emerged from this analysis. First, unlike conventional wisdom, the convective component shows weak northward propagation and grows and decays in situ during the evolution of active and break phases, while the northward propagation of the monsoon ISO is largely achieved by organized movement of the stratiform component. Second, the trademark meridional dipole pattern of total rainfall between the monsoon trough zone and the southern equatorial Indian Ocean also arises largely from the contribution of stratiform anomalies. As the northward propagation of the monsoon ISO is known to be due to the anomalous response of the atmosphere to heating in the presence of mean easterly vertical shear, modification of the vertical profile of heating due to a contribution from stratiform rain could influence the northward propagation of the monsoon ISO. This hypothesis is tested using a simple global atmospheric circulation model to study the response of the convective and stratiform heating profiles on the modification of the mean condition. Modification in the large-scale response of the atmosphere as a result of proper specification of convective and stratiform heating anomalies indicates that the presence of stratiform heating favors the northward propagation of the heat source thereby facilitating the positive feedback leading to northward propagation of the monsoon ISO. These results underline the importance of simulating the partitioning of convective and stratiform rain by cumulus parameterization in climate models if they have to get the space-time structure of the summer ISOs correct.

1. Introduction

[2] The northward propagating boreal summer intraseasonal oscillations (ISOs) manifesting in the active and break spells of the summer monsoon represent an important mode of variability of the Asian summer monsoon domain [e.g., *Yasunari*, 1979, 1980; *Sikka and Gadgil*, 1980; *Krishnamurti and Subrahmanyam*, 1982; *Lau and Chan*, 1986; *Wang and Rui*, 1990; *Lawrence and Webster*, 2001; *Goswami*, 2005]. Observations indicate that phases of the ISO travels to the north from south of the equator in the Asian monsoon region and can be identified with the northward propagation of the tropical convergence zone in the region [*Sikka and Gadgil*, 1980; *Krishnamurti and Subrahmanyam*, 1982; *Webster et al.*, 1998; *Goswami*, 2005]. The amplitude of intraseasonal variability (ISV) is much larger than that of the interannual variability of the seasonal mean and is comparable to that of the seasonal cycle [*Waliser*, 2006], thus providing optimism for extended range prediction. While on one hand, the ISV influences predictability of the seasonal mean climate [*Goswami and Ajaya Mohan*, 2001], it also influences weather predictability by modulating the frequency of occurrence of synoptic events such as lows and depressions [*Goswami et al.*, 2003]. The monsoon ISV has a large spatial scale, an example of which is illustrated in Figure 1 where a phase composite of the dominant ISO and its northward propagation is seen from the Global Precipitation Climatology Project (GPCP) [*Huffman et al.*, 2001] precipitation. Thus, boreal summer ISV represents a key building block of the Indian monsoon.

[1]Indian Institute of Tropical Meteorology, Pune, India.
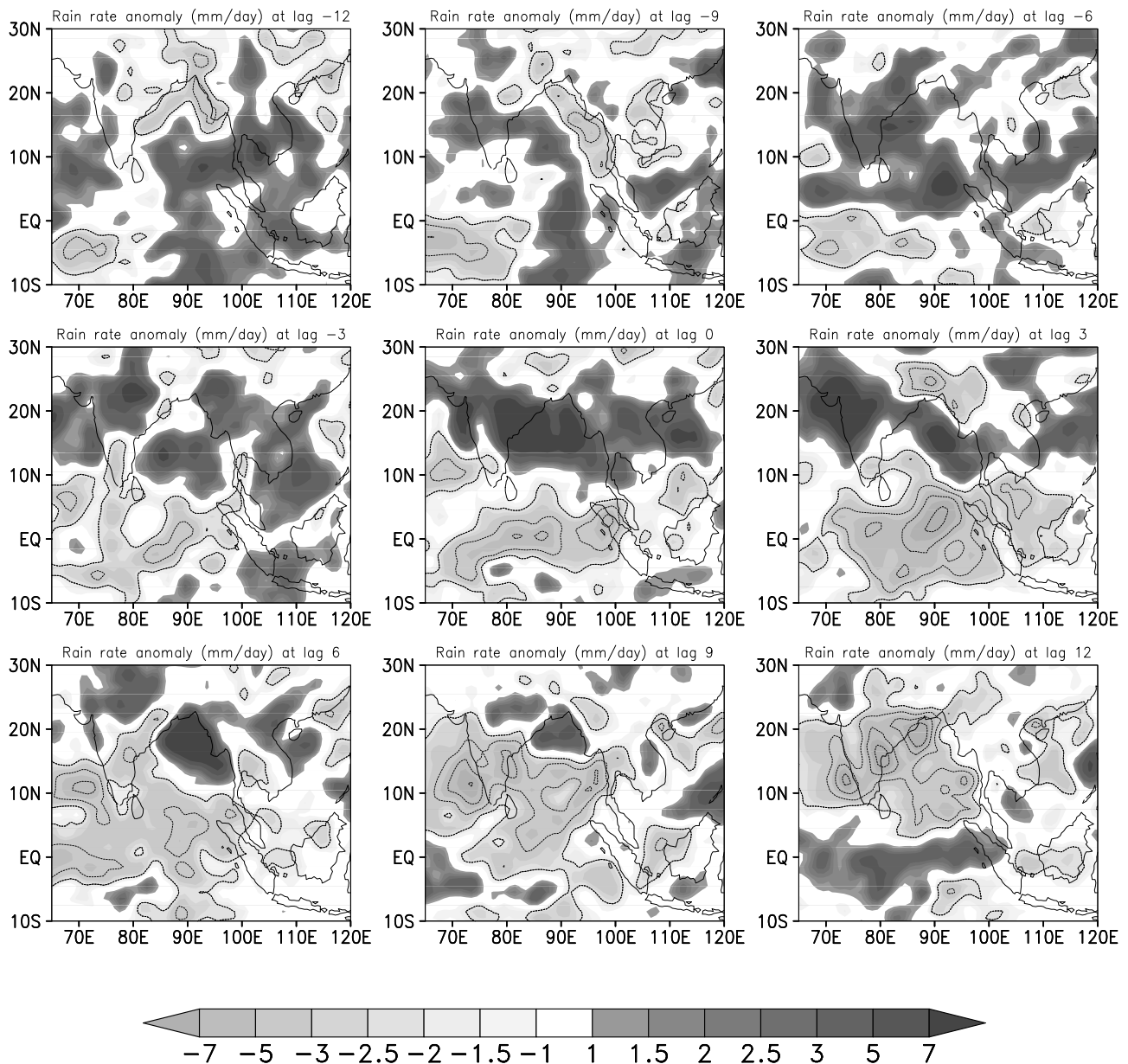[2]KlimaCampus, University of Hamburg, Hamburg, Germany.

Figure 1. The lag composite plots (of active spells) showing the ISO spatial structure and northward propagation from GPCP daily $1° \times 1°$ data. The reference time series is the IMD daily $1° \times 1°$ rainfall data over central India $(15-25°N, 70-85°E)$. The composites are taken when the active spells (constructed from a standardized anomaly) are ≥ 4 days (see text).The plots are smoothed using a 1-2-1 spatial smoothing. The negative anomalies are contoured (GPCP rainfall in mm d^{-1}).

[3] The conceptual models of ISO to date are to some extent able to explain its scale selection, its vertical and horizontal structure, its northward phase propagation, the role of air-sea interaction, the role of the land surface, and various other factors that influence the ISO [*Drbohlav and Wang*, 2007; *Hsu et al.*, 2004; *Sui and Lau*, 1989; *Webster*, 1983; *Goswami and Shukla*, 1984; *Gadgil and Srinivasan*, 1990; *Srinivasan et al.*, 1993; *Goswami*, 1994; *Kemball-Cook and Wang*, 2001; *Fu et al.*, 2003; *Bhaskaran et al.*, 1998; *Jiang et al.*, 2004]. However, the realistic simulation and prediction of monsoon ISO still remains a challenging and open problem for the dynamical modelers. One of the unsettled problems in this regard is the handling of the vertical heating profile to explain the space-time structure of the ISO, the model simulation of which is sensitive to the treatment of the vertical structure of heating [*Lau and Peng*, 1987]. Any dynamical theory of the ISO has to include the role of latent heating (i.e., moist static energy) in the tropics while constructing the vertical profile of diabatic heating in the models. As described by *Wang* [2005], this heating profile is often assumed to be that of a convective one (i.e., heating perturbation increases with height to a maximum near the midtroposphere and again decreases above) in the current theories of monsoon intraseasonal oscillation. Some early observation study indeed confirmed the convective diabatic heating profile in the "hot towers" of convection in
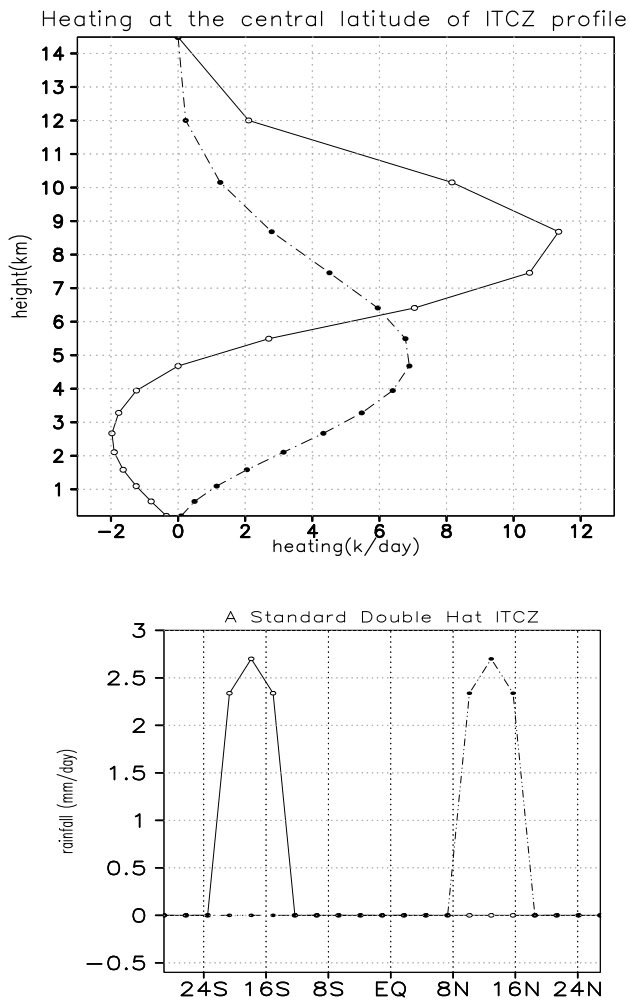
Figure 2. (a) The standard vertical heating profiles constructed for 100% convective contribution (dotted curve) and 70% stratiform contribution (solid curve). (b) The latitudinal variation of the total rain rate anomaly (mm d^{-1}), averaged over all longitudes, used for the construction of these heating profiles. This rain rate profile is referred to as the hat ITCZ profile in the text.

the equatorial belt and tropics [*Riehl and Malkus*, 1958; *Riehl and Simpson*, 1979]. However, as shown by some recent studies [e.g., *Stano et al.*, 2002; *Houze et al.*, 2007], a significant fraction of rainfall during the monsoon season over the Indian subcontinent is contributed by stratiform rainfall. The stratiform rainfall, falling from the large-scale extension of the cloud anvils from these hot towers (also referred to as "mesoscale convective systems") can have a very large spatial scale and can have thermodynamic properties entirely different than the convective counterpart [*Houze*, 1982]. Although the existence of both stratiform and convective rainfall is known to the tropical meteorologists [*Malkus and Riehl*, 1964; *Ramage*, 1971], the theories of monsoon ISOs developed so far do not split the role of stratiform and convective heating in determining the space-time structure of monsoon ISO. In particular, the role of these heating profiles in modifying the northward phase propagation of the monsoon ISO is not included in the most recent theories of northward propagation of ISO [e.g., *Jiang*

et al., 2004]. While most theories of convectively coupled tropical oscillations highlight a strong interactive role played by large-scale dynamics and heating, they remain relatively passive in assessing the role of variation of vertical profiles of diabatic heating in selection of the space-time structure of these oscillations.

[4] Many theoretical and modeling studies, on the other hand, describe the response of large-scale dynamics and Madden-Julian Oscillation (MJO) to the variation of the vertical profile of diabatic heating due to the presence of the stratiform and convective heating profile [*Hartmann et al.*, 1984; *Houze*, 1982, 1988, 1989, 1997; *Houze et al.*, 2007; *Lin et al.*, 2004; *Schumacher et al.*, 2004; *Lee et al.*, 2009]. These studies are based on the measurement of realistic latent heating estimates from the Tropical Ocean–Global Atmosphere Coupled Ocean-Atmosphere Response Experiment (TOGA-COARE) field experiment, some other regional observations [e.g., *Ogura and Cho*, 1973; *Mapes and Houze*, 1992, 1995; *Lin and Johnson*, 1996; *Chen et al.*, 1995; *DeMaria*, 1985], and currently from the Tropical Rainfall Measuring Mission (TRMM) satellite measurements on a global scale [*Tao et al.*, 2006; *Simpson et al.*, 1988]. The estimates based on these observations give a clearer picture of vertical profile of stratiform and convective heating. As an example, a convective and a (mostly) stratiform heating profile are shown in Figure 2a, and it may be seen that they differ in the magnitude (as well as sign) of heating at different vertical levels. The stratiform anomaly profile is associated with the heating at the upper level (~300 hPa) and cooling near the surface, whereas the convective heating profile is associated with the heating at the midlevel within the tropopause. A gross understanding from these studies is that the large-scale climate may be modulated in a significantly different manner for the two types of heating profiles. Such modulations, thus, can have significant impacts on the monsoon ISO, the existence of which, as described here, is grossly dependent on large-scale basic state of the atmosphere. However, to date, there is no comprehensive observational study of the spatial structures of convective and non-convective rain rates associated with phase propagation of monsoon ISO, their role in forming the observed structure of subseasonal variability, and the role of vertical variation of heating on the monsoon ISO and its northward phase propagation. Therefore, in this paper, we address the following two important questions that were not addressed till now: (1) what are the observed large-scale characteristics of convective and nonconvective (defined to be completely stratiform as described in section 2) rainfall pattern (spatial distribution) in the context of the northward propagating monsoon intra-seasonal oscillation from the TRMM data and (2) does any difference in the heating profile (i.e., convective or stratiform) matter significantly for the northward phase propagation of the monsoon ISO? On the basis of evidence of the convectively coupled nature of monsoon ISOs with a strong relationship between monsoon intraseasonal oscillation in precipitation with that of large-scale dynamical parameters [*Chattopadhyay et al.*, 2008] and on studies of the role of vertical distribution of heating on MJO, we would like to hypothesize that a variation in the vertical profile of heating would have a significant impact in the

northward phase propagation of ISO through the modification of large-scale dynamics.

[5] The paper is organized as follows. The data used in the study and the simple model to test our hypothesis are briefly described in section 2. Results of our diagnostic study using the TRMM data and from our sensitivity study with the simple model are discussed in section 3. Conclusions are summarized in section 4.

2. Data and Model

2.1. Data

[6] The data set that we use here for the observation studies is taken from a TRMM-derived data set referred to as 3G68. This is a combination of TRMM products 2A12, 2A25, and 2B31 [*Haddad et al.*, 1997a, 1997b; *Iguchi et al.*, 2000; *Kummerow et al.*, 2001], which are downloadable from the TRMM open source site: ftp://trmmopen.gsfc.nasa. gov/pub. This is a global tropical data set (40°N–40°S, 0°–360°E) available from 1997 to present. For this study, the daily data from May–October for the years 1998–2007 is used. The data set has a resolution of 0.5° × 0.5°, and the 3G68 product includes 24 h of hourly grids into a single daily file [*Kummerow et al.*, 2000; *Stocker et al.*, 2001; *Lin et al.*, 2004; *Nakazawa and Rajendran*, 2004]. For more information on this data set we also refer to the following Web site: http://rain.atmos.colostate.edu/CRDC/datasets/ TRMM_3G68.html. This data set gives the total number of pixels, number of rainy pixels in a 0.5° × 0.5° grid, rain rate estimates in the grid box in mm h^{-1} from the rainy pixels and the percentage of convective rain by separating the convective pixels and thereby estimating the convective rain rate. The convective rain rate is estimated in the 3G68 data using the 2A25 algorithm [*Iguchi et al.*, 2000] taken from TRMM. The 2A25 algorithm estimates the true effective reflectivity factor Z_e at 13.8 GHz at each precipitation radar resolution cell from the measured vertical profiles of reflectivity factor Z_m. The rainfall rate R is then calculated from the estimated Z according to the power law: $R = aZ_e^b$ in which the parameters a and b are both functions of the rain type and the heights of the 0°C isotherm and storm top. Effects of rain type, presence or absence of a bright band, the phase state, the temperature, and the difference in terminal velocity from changes in the air density are taken into account in 2A25 algorithm. We assume that the rain from the nonconvective pixels (if present) comes from the nonconvective anvils, arising from the extended anvil of subgrid-scale hot towers, that we describe here as stratiform in this paper. This definition of stratiform differs from that of *Houze et al.* [2007] where the stratiform component, in addition to its origin in the anvil structure of mesoscale convective systems, also has a large spatial scale (i.e., large number of grids) due to the extension of the anvil. Here we define stratiform and convective rain rate within the dimension of 0.5° × 0.5° grid box. The presence of both stratiform and convective in a grid box is justified since the dimension of the grid box (~2500 km^2) is much larger than the spatial scale of convective cells (~100 km^2). However, this does not contradict *Houze et al.* [2007] or the accepted definition of classical radar-sounding terminology because the nonconvective rainfall (as may be seen in section 3) shows large-scale organization in the subseasonal scale

quite similar to the broader and lower amplitude echoes (classified as stratiform) in the contoured frequency by altitude diagrams in radar meteorology. This paper also assumes that the significant (or total) contribution to the total rain comes from the stratiform and the convective components only without any subclassification of convection as "deep" or "shallow" as done by *Schumacher et al.* [2004]. This is because of the fact that the observed large-scale organization of the nonconvective rain rate as will be discussed (e.g., Figures 5 and 7) fit to the theory of existence and properties of stratiform rain in the tropics. On the other hand various studies on the interannual and monthly time scale in the global tropics (based on TRMM data) [e.g., *Schumacher et al.*, 2004] do confirm the existence of large stratiform fraction (during monsoon season). It is well known that the spatial mode of variability on the ISO and interannual scale do have common dominant modes; hence, organized existence of stratiform rain is also possible on the ISO scale. Thus, existence of stratiform rain is assumed in a grid box along with convective rain in this study. We calculate the stratiform percentage from the data by subtracting the convective component from 100. First, a 3-day running mean of the data from May to October of 1998–2007 is created which actually covered the entire global tropics. Next using the total smoothed rain rate (RR) (mm h^{-1}) (the rain rate unit, mm h^{-1}, is occasionally converted to mm d^{-1} in the plots by multiplying the rain rate from TRMM 3G68 with 24, as the frequency of observation is once daily) value we obtained the convective rate from the given convective percentage (C) and the stratiform rain rate from stratiform percentage (taken as $100 - C$), i.e., convective rain rate = RR × C% and stratiform rain rate = RR × $(100 - C)$%, at each grid for each day. Finally, a 10-year long-term mean (climatology) is obtained for each day from the smoothed data for each of the convective, stratiform, and total rain rate components.

[7] Before using the 3G68 data to see the convective and stratiform components, we compare the 3G68 data with the Moderate Resolution Imaging Spectroradiometer (MODIS) cloud optical depth data (COD). The COD may be used as a measure of convection. Linear correlation of the area-averaged MODIS COD and 3G68 rainfall daily data (both total and convective components during June–August) over the Indian subcontinent (70°–90°E, 15°–30°N) and Indian Ocean (70°–90°E, 5°S–5°N) are computed for the years 2002–2007. The correlation (though it varies year to year) is highly significant (result not shown) both over land and ocean (though over ocean the correlation is higher). Thus, the 3G68 rain rate may be used to compute the convective and stratiform rain rate. In order to examine the large-scale organization of the total rain rate from TRMM, RR, during evolution of an active and break phases of the monsoon ISO and to compare such patterns with those obtained from other data sets such as the GPCP (Figure 1), a standard lag-lead pattern composite is created with the GPCP rainfall with respect to a reference time series obtained by averaging over Central India (15°N–25°N, 70°E–85°E) from the India Meteorological Department (IMD) gridded rainfall data [*Rajeevan et al.*, 2006]. The spatial patterns composite and the lag-lead patterns (after subtracting the long-term mean) are produced after identifying the active and break spells from central India area-averaged IMD rainfall data
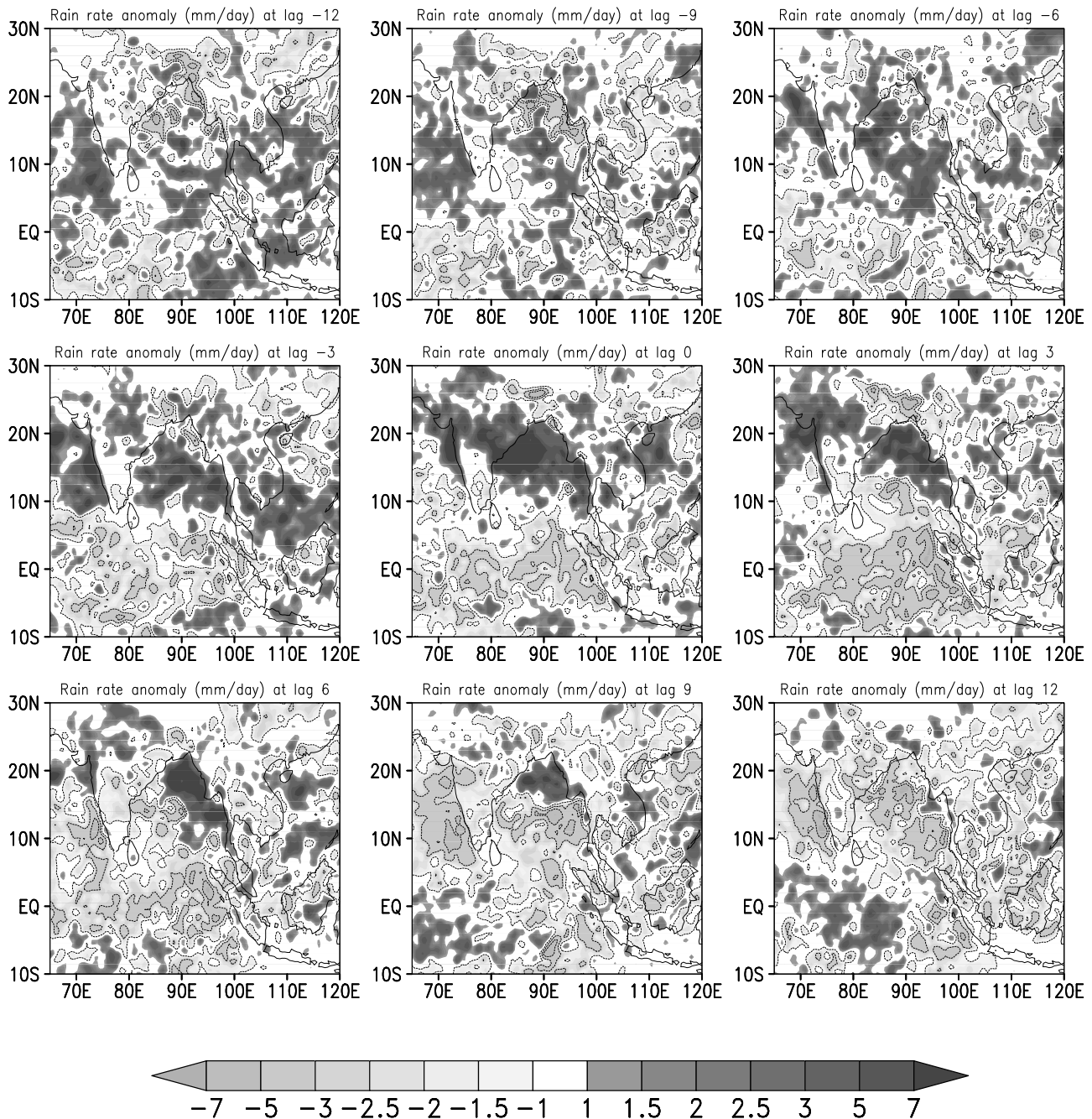
Figure 3. The active phase lag composite anomaly plot for the TRMM 3G68 total rain rate similar to Figure 1 (in mm d^{-1}). The plots are smoothed using a 1-2-1 spatial smoothing.

during 1 June to 30 September. The active period is identified as when the standardized rainfall anomaly is greater than 0.8 for 4 days or more and average anomalies during these days are greater than 1.0. (Sometimes it is observed that the rainfall variation is quite large in a particular day even during the peak active or peak break phase. In order to accommodate such large variation during the spells, the variation of ±0.8 standard deviation for individual days (which corresponds to at least 4 mm d^{-1}) and ±1 standard deviation for continuous 4 days is chosen.) The break period is identified as when the standardized rainfall anomaly is less than −0.8 for 4 or more days and average anomalies during these days are less than −1.0. Using this method,

21 break spells and 24 active spells are identified from IMD data during 1998−2007 (tables not shown). The lag-lead composite of the active and break phases are plotted by fixing the lag 0 as the central day of the established active and break phases and thereby picking up days backward (−12, −9, etc.) and forward (9, 12, etc.) from this central day to get the lag composite. The composite in Figure 1 from GPCP [*Huffman et al.*, 2001] for the same period as TRMM data (1998−2007) for active composite and the similar composite in Figure 3 from TRMM may be compared for the active phase evolution patterns. Typical northward propagating character of monsoon ISO is evident from these patterns. More features of these plots will be

formally discussed in section 3.2. Subsequently, the similar composites are plotted for stratiform and convective rain rates, and further discussions from the observation regarding northward propagation are also presented in section 3.

[8] The other part of this analysis requires the construction of the vertical heating profile from the TRMM rainfall data that will be used in the model. Two vertical heating profiles are constructed from TRMM long-term mean data. These profiles will represent two broad classifications: convective and stratiform. The dotted curve as shown in Figure 2a is termed C100, which means the diabatic heating is due to a complete convective rain rate. The other profile (solid curve) is termed as S70 which implies the diabatic heating has a 70% contribution from stratiform rain rate and 30% convective rain rate. Such a choice of profile is made in order to see the clear difference in response from the model. These are constructed in a similar way as that of *Schumacher et al.* [2004] and the order of temperature perturbation in the profile is similar to that of Figure 3b of *Schumacher et al.* [2004].

2.2. Model and Its Configuration

[9] On the basis of the observational study, a simple global atmospheric circulation model, Portable University Model of the Atmosphere (PUMA), is used to perform some experiments by modifying the vertical heating profile in the dynamical core of the model. PUMA is an atmospheric circulation model consisting of the dynamical core together with Newtonian cooling, Rayleigh friction, and hyper diffusion. It was developed at the University of Hamburg [*Fraedrich et al.*, 2005a] as a research and teaching model for the community. The model is available for download at http://www.mi.uni-hamburg.de/puma, with source codes, manuals, graphical user interface, postprocessor and tools; besides PUMA, there are shallow water models for atmosphere and ocean and the Planet Simulator as a coupled system [*Fraedrich et al.*, 2005b].

[10] Our aim is here to see the zonally asymmetric response of the large-scale dynamics (large-scale wind shear and vertical profile of wind and vorticity) that take an important role in the northward phase propagation of the monsoon intraseasonal oscillation. To accomplish this task, an aqua planet version of PUMA without any moisture variable (i.e., only a dry dynamical core) is used for these experiments with T42 horizontal resolution ($128°$ longitude by $64°$ latitude) having a grid spacing of $\sim 2.9°$ in latitude and longitude. The model is configured to have 18 vertical sigma levels with an arrangement of equal sigma level spacing. This arrangement places most of the vertical levels within the tropopause. The time step of the model is 30 min. The time scale of Rayleigh friction is maximum at the 4th level ($\sigma = 0.806$) from the bottom with a value of $(2.6\ d)^{-1}$ and decreases both above and below. The vorticity and divergence are relaxed toward state of rest with the above mentioned time scale. The time scale of Newtonian cooling increases from a value of $(1.4\ d)^{-1}$ at $\sigma = 0.972$ (the bottom level) to a constant value $(30\ d)^{-1}$ at $\sigma = 0.306$ and above (up to the topmost level $\sigma = 0.028$). The evolved temperature T is relaxed toward a restoration temperature profile, T_R, prescribed from the initial time with the above mentioned time scale. The T_R profile varies with latitude and

height and is dependent on equator to pole (DTEP) and North Pole to South Pole temperature gradients (DTNS). The values of DTEP and DTNS are taken as $53°C$ and $-70°C$, respectively, for all the model experiments (default choice in the model).

[11] The model is used to see the time-dependent, nonlinear zonally asymmetric response of the dynamical parameters to an idealized vertical heating profile arising from a narrow zonal rainfall band over the land (ideally over the monsoon trough zone (MTZ)) which we will denote as an idealized Intertropical Convergence Zone (ITCZ) over land with a hat profile (Figure 2b). On the other hand, when the land ITCZ is active (i.e., there is a positive rainfall anomaly on the intraseasonal scale) there is a negative rainfall anomaly around the southern equatorial Indian Ocean. This structure is the so-called "dipole" pattern present during active phases (see lag 0 plot, Figure 1), and it reverses its anomaly pattern during a break. The large-scale variability and the structure of monsoon ISOs are essentially represented as the fluctuation in the ITCZ. Hence, we choose a rainfall distribution that has a hat profile of positive anomalies with the spatial scale of 3 grids similar to a realistic ITCZ over northern tropics (taken to be centered around $13°N$) and negative anomalies over the southern equatorial Indian Ocean (taken to be centered around $18°S$) corresponding to an active monsoon condition (Figure 2b). The choice of such centering of the hat profiles is based on the seasonal mean position of the ascending and descending branch of the Hadley cell in the model during July (discussed in section 3.3). The positive and negative heating anomalies associated with the rainfall anomalies in the Hadley cell are termed as heat source and heat sink, the strength of which is assumed to be proportional to the rainfall anomalies. The positive heating profiles (i.e., heat source, Q) for C100 and S70 are shown in Figure 2a and are constructed corresponding to the maximum rainfall value at the central latitude of the hat profile taken to be ~ 3 mm d^{-1} above the long-term mean (a typical value found in the TRMM data for composite active spell amplitude, area averaged over the MTZ). The heat sink has a similar profile but with a minus sign, i.e., $-Q$. The two other latitudes which have slightly lower rainfall value in the hat profile (on either side of the maximum value in Figure 2b) have the similar profile but the magnitudes of temperature perturbation at each vertical level are reduced in a linear fashion corresponding to the rain rate value. The anomalous heat source and heat sink (i.e., the temperature perturbations constructed on the basis of S70 and C100 profile) will be collocated on these hat profiles to see the large-scale response of wind during an active or a break phase.

2.3. Design of Experiments

[12] The model is designed to run in 2 modes, the first one being the control run (CTRL), and the other one is called the perturbation run (PERT). In the CTRL run the model is integrated freely from the stably stratified initial state with a planetary vorticity and with a prescribed annual cycle of temperature. The annual cycle has a constant part and a varying part (as a function of the Julian days). All the experiments are performed when the temperature annual cycle corresponds to the 1 July condition as prescribed in the model. The model gets stabilized (the model is assumed to be stable when all the large-scale features in the model (north
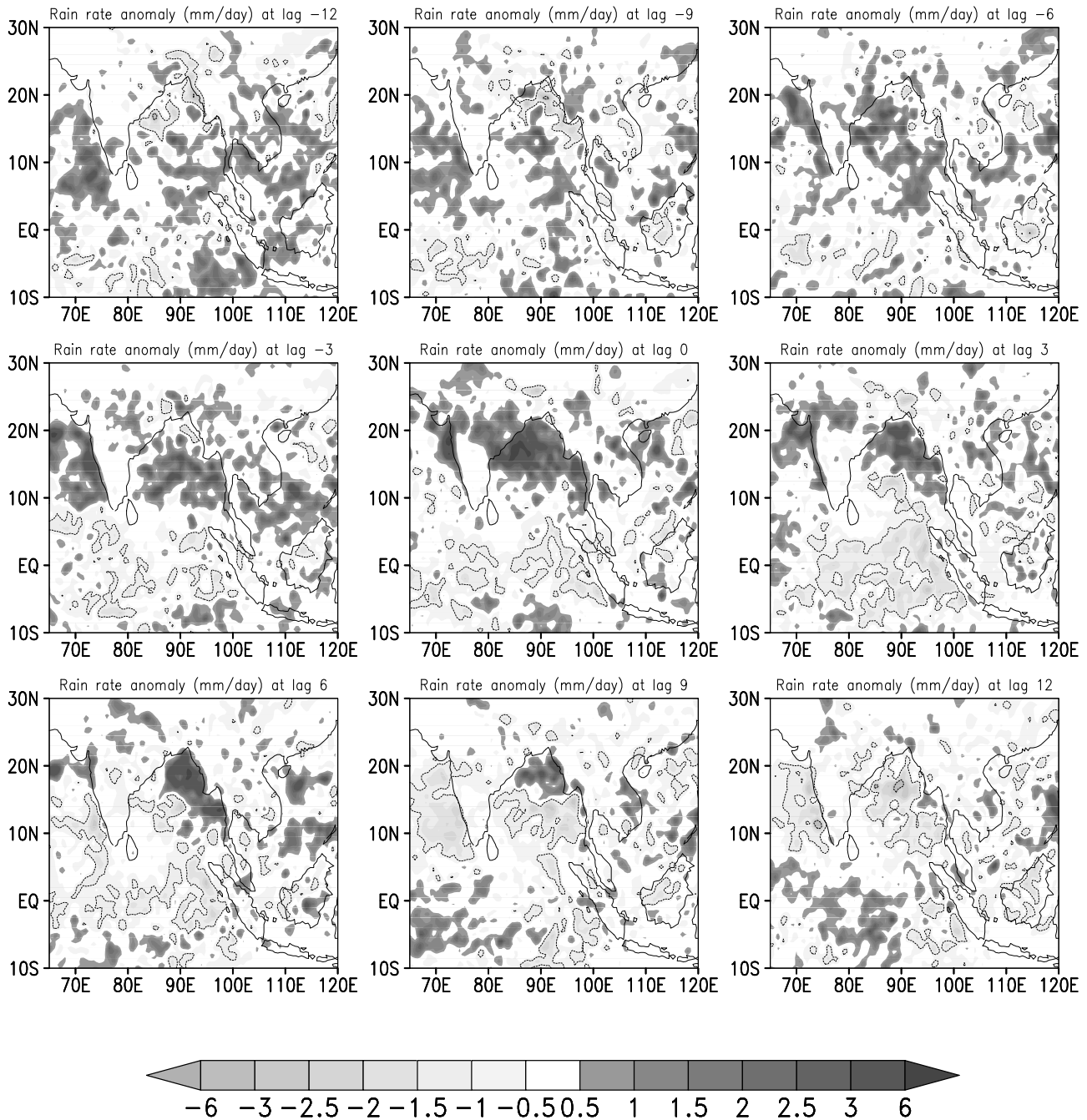
Figure 4. Same as Figure 3 but for convective rain rate (mm d^{-1}) obtained from the convective percentage in the data.

south temperature gradient, subtropical jets, etc.) got well established, and the global mean wind kinetic energy does not grow monotonously) within 25 days with the subtropical jets getting established due to north to south and top to bottom temperature gradients (because of the annual cycle and the thermal wind balance). For the CTRL run the model starts integrating from 16 June with the prescribed initial condition as described here, and after it gets stabilized on 1 July, the run is continued for another 30 days. For the PERT run, the diabatic heating profile (vertical variation of temperature perturbation) is added to annual cycle on 1 July and is continued for another 30 days as earlier. The PERT run is

carried out with two temperature perturbations, C100 and S70, as shown in Figure 2a. For both the cases the zonal asymmetry of the hat ITCZ profile is maintained for all the longitudes (i.e., the perturbation heating is applied only in the latitudes that incorporate the hat profile). Both the PERT and CTRL runs are continued in such a way that at each time step the lowest mode (wave number zero) of vorticity, divergence, surface pressure, and temperature is added to their evolved value (after applying a standard Robert-Asselin time filter). This is done in order to force the model continuously at each time step with the lowest zonal symmetric component of the initial values so that a component of the perturbation is
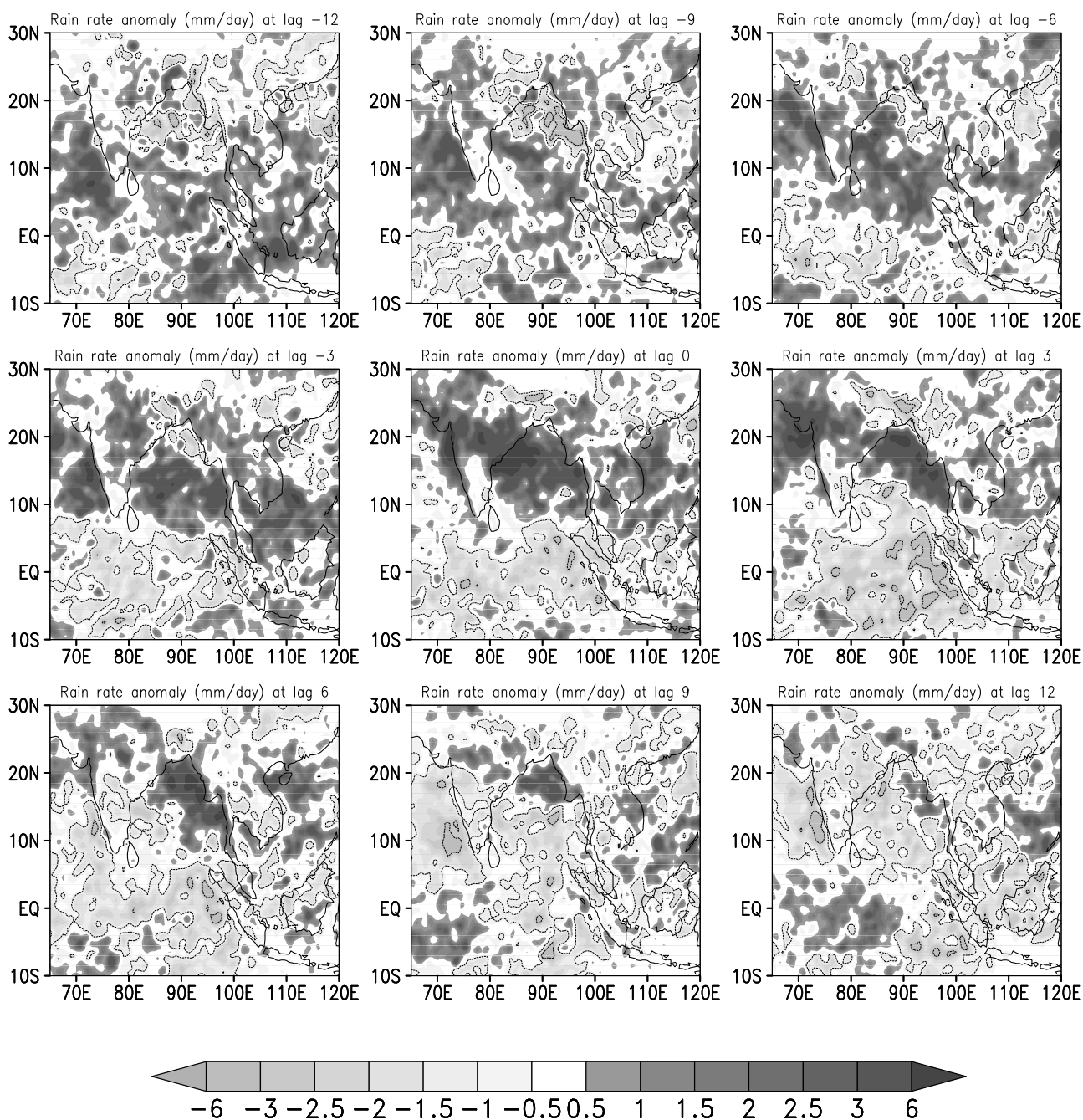
Figure 5. Same as Figure 3 but for stratiform rain rate (mm d^{-1}) obtained from the stratiform percentage (taken as 100 minus the convective percentage) in the data.

always present at each time step and ensuring that it is not damped out.

[13] For all the experiments, the PERT run and the CTRL run get stabilized around 25 days from 1 July, and hence, the $26-31$ July day average value from 1 July is considered to be the model response. This 6 day averaging is done to smooth out very high frequency fluctuations. The aim of all these arrangement is to show the modification in the response of large-scale dynamical parameters that favor northward propagation when we use stratiform (S70) heating profile as heat source ($+Q$) and heat sink ($-Q$) as compared to the traditional case, for example, where only the convective heating profile (C100) is used (as in the accepted theories of

ISO) as heat source and heat sink. The results of these experiments will be discussed in section 3.3.

3. Results and Discussion

[14] The generalized structure of summer monsoon convection over the Indian region and the Himalayan region for the years 2002 and 2003 has been studied in detail by *Houze et al.* [2007] using the TRMM data. They documented in detail the deep, wide, and intense convective and stratiform echoes having various horizontal scales present over the Indian region during these two seasons. They stressed on the role of monsoon depression in providing the large-scale
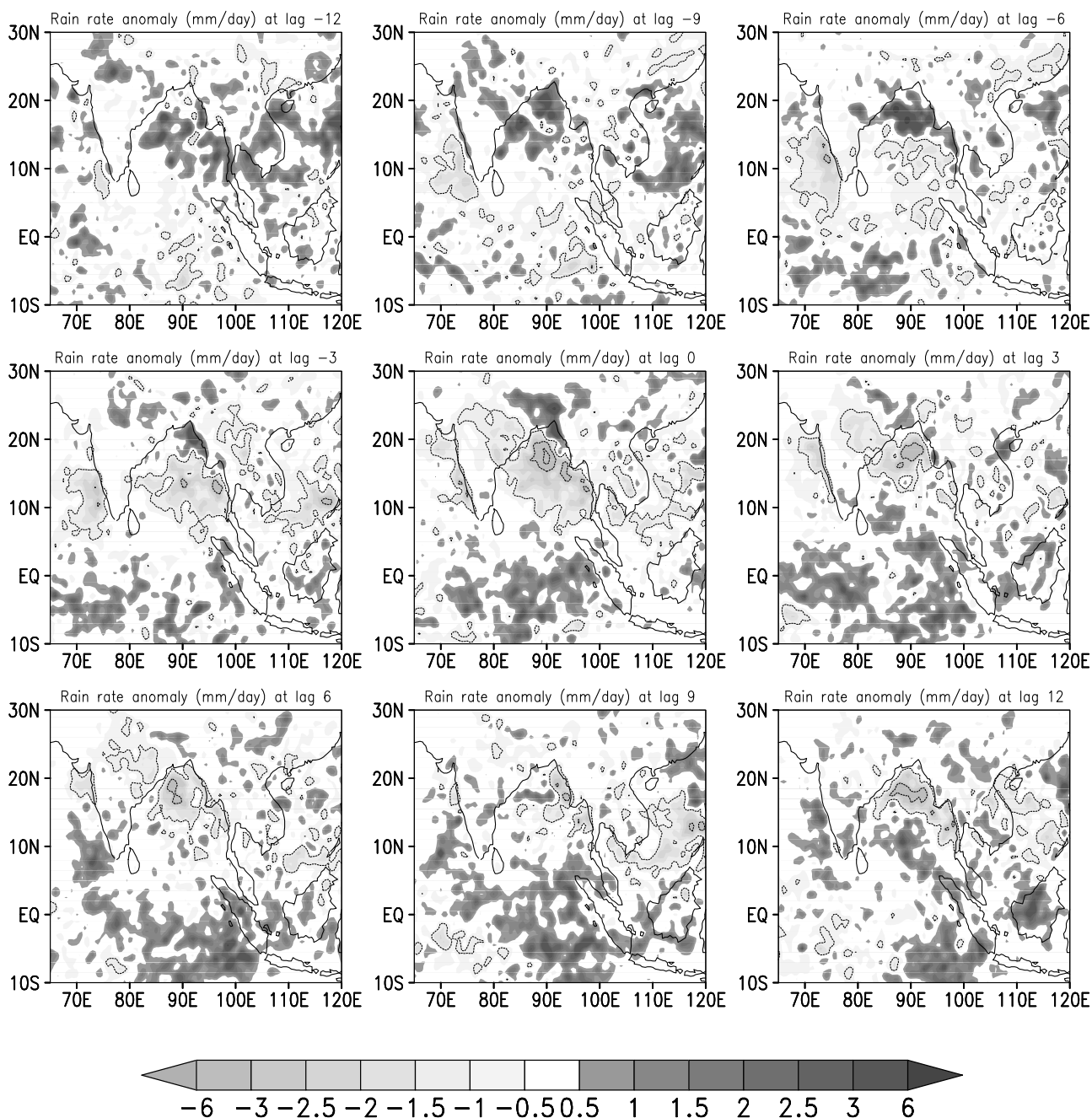
Figure 6. Same as Figure 4 but for break phase composites for the convective rain rate (mm d^{-1}); i.e., the lag composites are plotted for the selected break spells (see text) (in mm d^{-1}).

background environment in the development of convective instabilities in the mesoscale to the large-scale stratiform echoes. As the relative contribution of deep convection and stratiform convection to total rainfall during different phases of boreal summer ISO has not been documented, in sections 3.1 and 3.2 we shall present the composite and large-scale features of the monsoon intraseasonal oscillation using the TRMM convective and stratiform rain rates.

3.1. Observed Spatial Pattern of Monsoon ISO From TRMM 3G68

[15] The lag composite technique as discussed in section 2.1 is used to plot the spatial structure of the total rain rate from

TRMM with reference to active and break spells identified from the reference time series over central India (15−25°N, 70−85°E) constructed from the IMD data (the spells are same as used for GPCP plot in Figure 1). The plot is shown in Figure 3. The rain rate is plotted from lag −12 to lag +12 with an interval of 3 days. In order to highlight the large-scale organized component, the composited anomalies are slightly smoothed using a 1-2-1 filter both in the east-west and north-south directions. The lag 0 is the phase when the anomaly pattern (active) is prevalent and most organized over central India. The southeast to northwest orientation of the positive anomaly is seen similar to that in Figure 1. The northward and eastward propagation is also seen with the positive anomaly
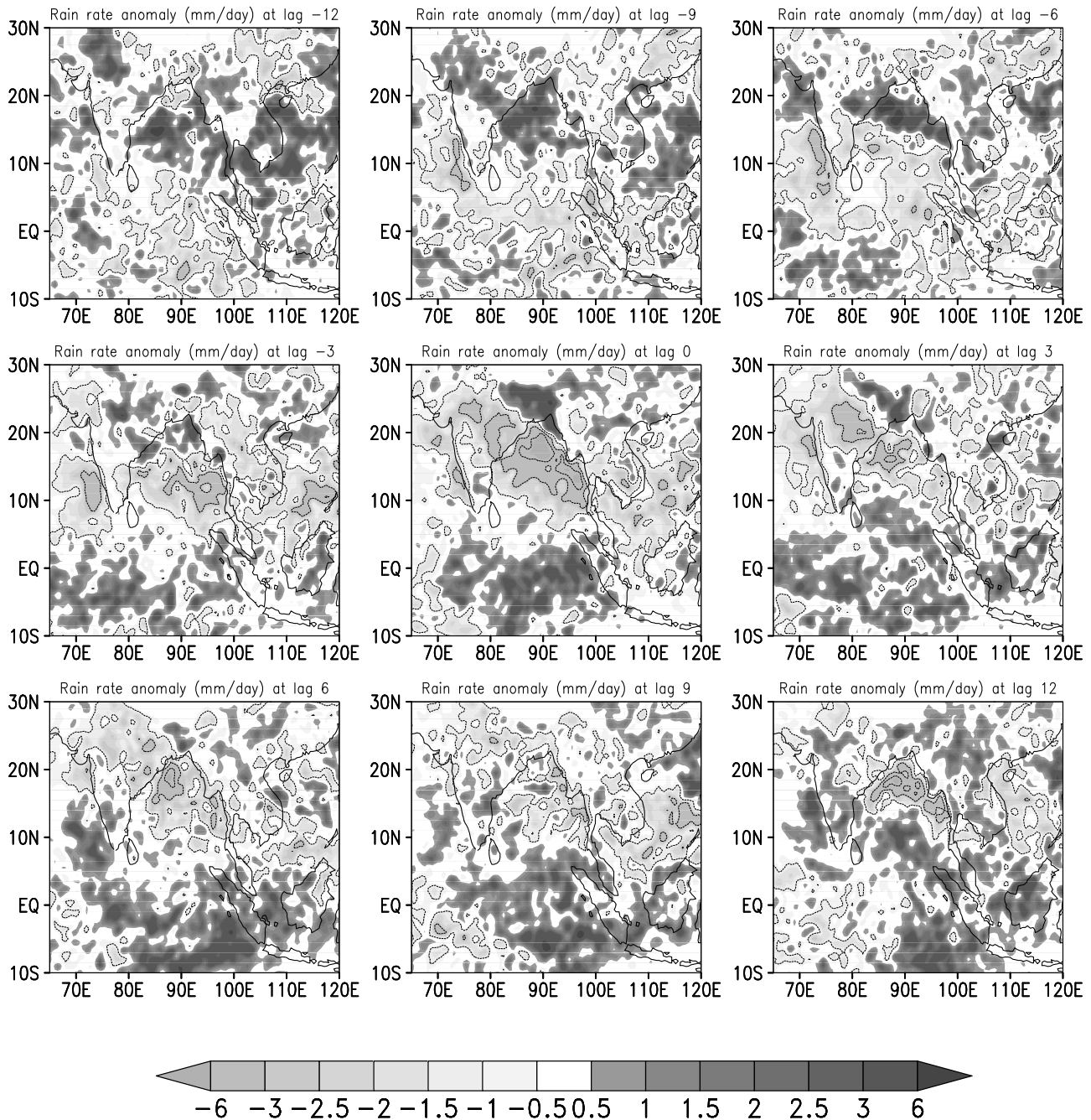
Figure 7. Same as Figure 6 but for the break phase composites for the stratiform rain rate (mm d^{-1}).

forming and organizing over the Arabian Sea and the Bay of Bengal from lag −12 and moving toward land peaking at lag 0. Thereafter, it moves eastward and weakens, and the negative rainfall anomaly moves in a similar fashion. This plot confirms various features of large-scale northward phase propagation (e.g., north-south dipole structure, lack of rainfall over northeastern India and the Tamil Nadu coast at lag 0, large-scale rainfall over the Bay of Bengal) from the TRMM 3G68 data. Similarly, the lag composite plot when there is a break over central India at lag 0 is seen to give similar northward phase propagation in the large scale (figure not shown).

[16] The rainfall is then partitioned to the convective and stratiform component by multiplying the corresponding

percentage (also supplied in the data) to the total rain rate. The lag-lead phase composites for the convective and the stratiform components are shown in Figures 4 and 5 with respect to an active phase. The composite technique is similar to the technique discussed in section 3.1. In both of these plots the seasonal mean is removed to get the intraseasonal fluctuation, and the anomalies are slightly smoothed as in Figure 3. In Figure 4 as we approach lag 0 from lag −12, the convective organization (large-scale appearance of maximum positive anomalies) increases, and before becoming maximum in central India at lag 0, the convective organization and intensity increases enormously over the Bay of Bengal at lag −3. The west coast of India also gets strong convective organization and
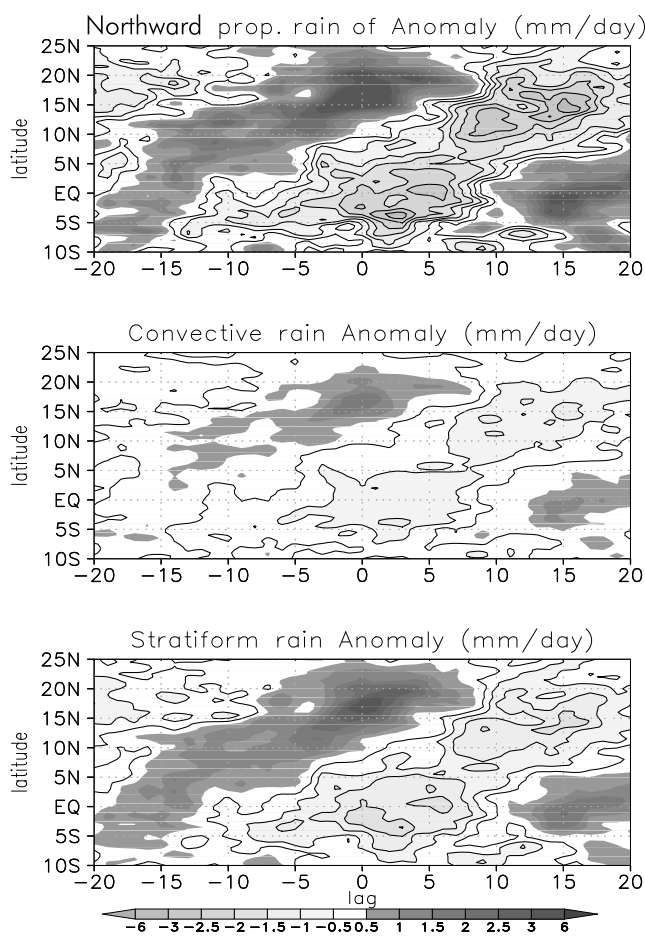
Figure 8. Hovmoller diagram for the northward propagation during active phases: (top) the propagation for total rain rate (mm d^{-1}), (middle) the propagation for convective rain rate (mm d^{-1}), and (bottom) the propagation for stratiform rain rate (mm d^{-1}).

intensity. As the convective anomaly increases over central India, it decreases over the Bay of Bengal and the Arabian Sea. One important feature of the convective rain rate anomalies around an active condition is that they seem to grow in situ without any perceptible northward movement (refer to Figure 8, also discussed in section 3.2). Another important feature to be noted for the spatial plot from lag 0 is that the north-south dipole type structure (refer to lag 0 spatial plot of Figure 2) is not prominent with the absence (or very weak presence) of negative anomalies over the equatorial Indian Ocean (in lag −3, lag 0, and lag 3) and weaker organization of positive anomalies in the land ITCZ as compared to the total rain rate (shown in Figure 3). This is an important departure from the classical concept of the spatial pattern of active phases over this region. At the lag −3, lag −0, and lag 3, positive and negative convective anomalies are not well organized as compared to the stratiform counterpart or the total rain rate (Figures 5 and 3) around the subcontinental ITCZ and the oceanic ITCZ, respectively. Therefore, it is natural to ask, what causes this classical dipole structure seen in total rainfall (Figures 1 and 3) and alluded to in various earlier studies [e.g., *Sikka and Gadgil*, 1980]? Figure 5 will provide an answer to this apparent anomaly from the classical concept, which

plots the stratiform rain rate in a similar manner as that of the convective rain rate. It is interesting to note that the north-south dipole pattern is prominent in the composite of stratiform anomalies. For example, at lag 0, while there is an increase in stratiform organization over the Indian continent together with an increase in the convective component (Figure 4), there is also an organized decrease of the stratiform component over the equatorial Indian Ocean, thus giving the dipole structure of Figure 3. Hence, the traditional north-south dipole pattern in rainfall associated with the active-break phases is largely contributed by variations of stratiform organization rather than convective organization. We believe that this is a new insight not recognized so far. Another interesting feature of the stratiform composites is that they have a clear northward propagation which was absent in the convective anomalies (also discussed in section 3.2).

[17] The spatial composite of the convective and stratiform rain rate for the break phase over central India are plotted in Figures 6 and 7, respectively. The convective rain rate plot in Figure 6 indicates the appearance of negative rainfall anomalies over the ocean at lag −9 which propagates to land at lag 0. The negative and positive anomalies of the convective rain rate are, however, not well organized from lag −3 to lag 3 as compared to its stratiform counterpart in Figure 7. Also, similar to Figure 4, there is no clear northward propagation of convective anomalies, and, sim-
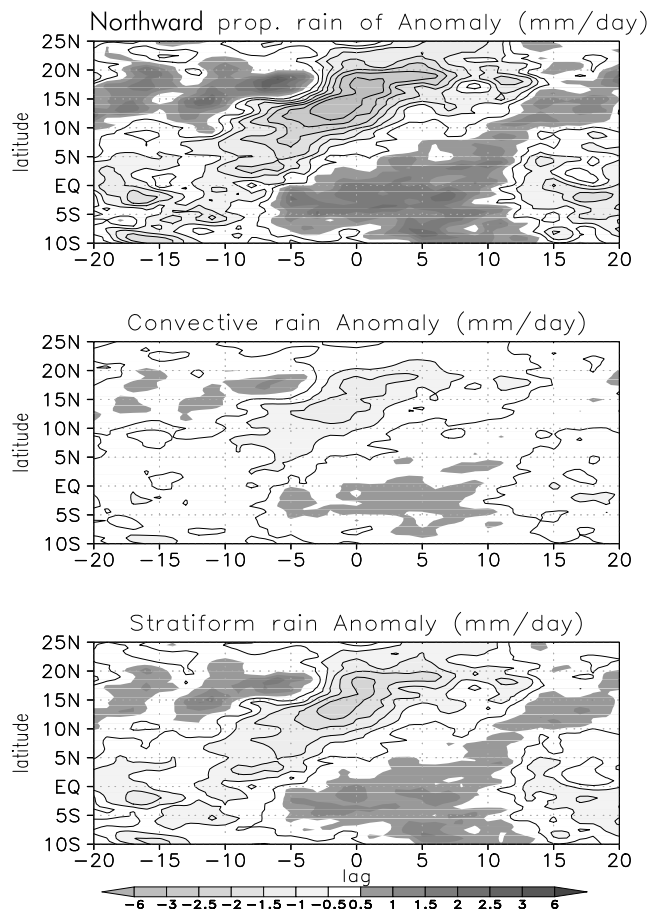

Figure 9. Similar as Figure 8 but for the propagation during the break phases.
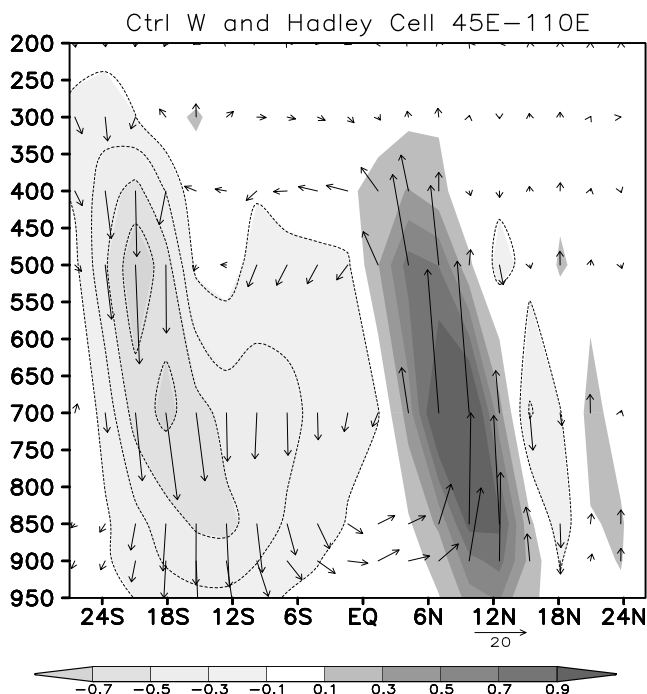
Figure 10. Plots to show the PUMA CTRL run. The meridional Hadley cell is shown as vectors and the mean vertical velocity ($\omega = -dp/dt$) is shown in shades. The omega is multiplied by a factor of 27×10^3 in the vector plot (omega unit is 10^{-3} hPa s^{-1}).

ilar to Figure 5, northward propagation of the stratiform anomalies is clear in Figure 7 even during breaks. Figures 4–7 convey that although the stratiform rain rate anomaly and convective rain rate anomaly coexist and when one increases the other also increases, the organization of these anomalies is quite different for the stratiform and the convective rain rate.

3.2. Northward Propagation of the Stratiform and Convective Rain Rate

[18] The latitude-time Hovmoller plot for northward propagation of the total rain rate and the convective and stratiform rain rates for the active and break phases are plotted in Figures 8 and 9. The plot is for the longitude averaged between $60–100°$E. The total rain rate shows the alternate phase propagation and the lag 0 shading anomalies over central India depict the propagation of the constructed active or break phases. For both the active and break phase composite, the phases propagate from $5°$S to $25°$N in about 20 days which corresponds to a propagation speed of $1.2°$ latitude per day. The convective and stratiform rain rate propagation for active and break phases, similarly, are shown in Figures 8 and 9 (middle and bottom). For both the active and break phase composites, the spatial organization of stratiform anomalies are more dominant than the convective anomalies. Also, the clear northward propagation of stratiform anomalies is apparent for both active and break phases. These plots indicate the differences in the convective organization of the rainfall anomalies during active and break phases. The stratiform rain rate (positive and negative anomalies) anomalies show more organized movements during both the break and the active

phase than the convective counterpart. The positive anomalies of the convective rain rate also show a weak sign of northward propagation in Figure 8 (middle) than the positive anomalies of stratiform rain rate (Figure 8, bottom). The lack of organized movement for the convective anomalies during both active and break phases may suggest that the convective rain evolves in situ, while the large-scale component of the total rain which is here attributed to be coming from a nonconvective origin shows clear northward propagation.

3.3. Model Simulation

[19] Having established that stratiform rain contributes in a significant way in the evolution of the monsoon ISO, in this section, we investigate how the atmospheric response is modified by the modification of the vertical structure of heating due to the appropriate mixture of convective and stratiform rain anomalies. In order to see what difference these heating distributions make to the atmospheric response and to bring out the contribution from the stratiform component of heating, we carry out two experiments. The model has a mean local Hadley cell during July with the ascending branch (ITCZ) around $13°$N and a descending motion around $18°$S (Figure 10). In the first experiment, we add an anomalous heat source ($+Q$) around $13°$N with an integrated heating that corresponds to a typical active rainfall anomaly
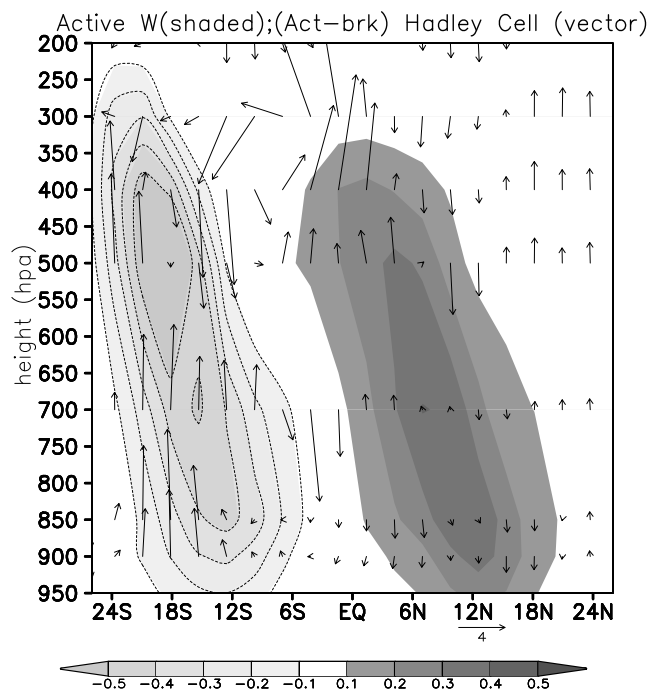

Figure 11. Vector plot of the anomalous Hadley cell for (active-break) profile using stratiform (S70) profile as anomalous heat sink at the southern equatorial Indian Ocean (MTZ) and anomalous heat source over MTZ (southern equatorial Indian Ocean) during active (break) phases, superimposed on vertical velocity (shaded) during the active phase, showing the locations of updroughts and downdroughts of mean Hadley cell (omega unit is 10^{-3} hPa s^{-1}). The omega is multiplied by a factor of 42×10^3 in the vector plot.

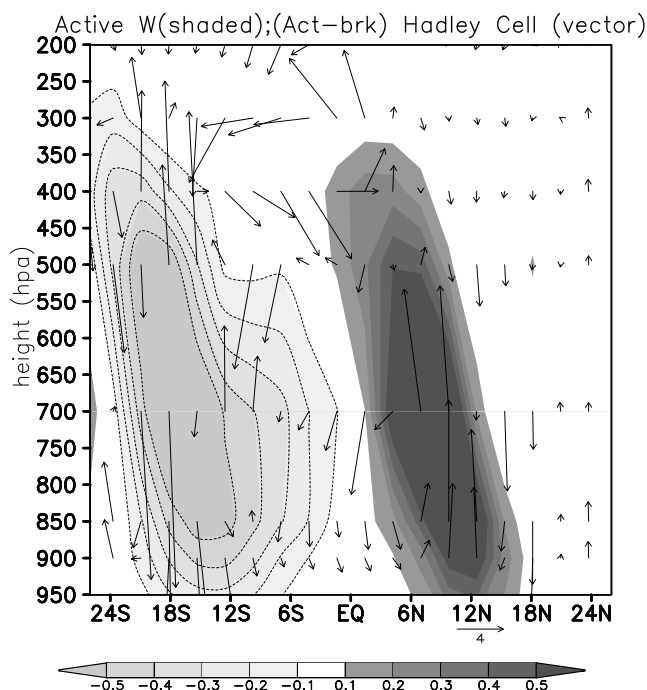## Active W(shaded);(Act−brk) Hadley Cell (vector)

Figure 12. Same as Figure 11 but for the case when anomalous convective (C100) heat source and sink is used during active and break phases (units same as Figure 11).

but that has a vertical structure corresponding to the contribution coming from 70% stratiform rain and 30% convective rain (i.e., S70). We also give an anomalous heat sink ($-Q$) at the south location with similar stratiform and convective components (S70). This represents an active condition. We also simulate the atmospheric response during break conditions by giving a heat sink ($-Q$) at the north and a heat source ($+Q$) at the south location using the same S70 profile. The difference in anomalous Hadley circulation during active and break conditions (active-break) is shown in Figure 11 (vectors) together with mean background vertical velocities during the active phase (shaded). It is noted from the (active-break) plot that in the upper atmosphere (above 500 hPa) for the active phases, anomalous Hadley circulation is strengthened significantly and the rising motion shifted to the north of the anomalous heat source located around $\sim13°$N by a couple of degrees. Also, it is noted that in the lower atmosphere (below 500 hPa), the upward motion to the south of the heat source (around $\sim13°$N) is weakened. This kind of response is expected to produce a larger convergence of boundary layer moisture to the north of the original heat source and help the formation of a new heat source to the north through the release of latent heat and thus effectively moving the heat source north ward [*Jiang et al.*, 2004]. Thus, the enhanced contribution of stratiform rain during active conditions is expected to facilitate the northward propagation of the rain belt.

[20] In order to isolate the role of stratiform component, we repeated the response of the atmosphere during active and break assuming that both positive and negative rain anomalies came entirely from convective rain (i.e., both heat source and heat sink are constructed using C100 profile). The difference in anomalous Hadley circulation during active and break conditions (active-break) if it were only convective

rainfall is shown in Figure 12 (vectors) together with mean background vertical velocities (shaded areas) during the active phase. It is clear that if it were heating arising from only convective rains, the largest ascending motion is collocated with the heat source, and hence, northward propagation of the heat source would not be facilitated. A comparison of Figure 12 and Figure 11 shows clearly that the stratiform rain anomalies lead to the northward shift of the ascending branch and hence to the northward migration of the heat source.

4. Conclusion

[21] Observation from the TRMM satellite and many modeling studies showed the role of stratiform clouds in modulating the dynamical response of the atmosphere. However, there has been no documentation of the spatial pattern of the convective and the stratiform rain rates during different phases of the northward propagating monsoon intraseasonal oscillation. We first compared the northward propagation and large-scale organization of the total rain rate anomalies from the TRMM 3G68 data corresponding to different phases of monsoon intraseasonal oscillations with those obtained from other products (e.g., GPCP). Using the same data we also have shown the pattern propagation of the convective and stratiform rain rate and its fluctuation during an active or break phase of monsoon. Over the Indian subcontinent and Indian Ocean, the stratiform fraction shows large-scale organization during both the break and active phases with larger amplitude of anomalies over certain region than the convective counterpart. It is also interesting to note that the northward propagation of organized anomalies during both break and active phases is largely contributed to from the stratiform fraction, while the convective fraction is not showing significant propagation of anomalies.

[22] An attempt is made to assess the role of the stratiform and the convective heating in modulating the phase propagation of the monsoon intraseasonal oscillations through a modeling study. A simple global spectral model of the atmospheric circulation known as PUMA is used for this purpose. As this model does not include dynamical moist feedback, such a simple model cannot have a realistic intraseasonal oscillation. However, it is still a nonlinear model that has a realistic large-scale dynamical basic state and hence could be a useful tool for studying the anomalous response of heat sources and sinks. We asked the following specific question. Could the modification of the vertical structure of the heating profile (due to significant contribution to the total rain rate by stratiform rain) modify the atmospheric response significantly to affect the northward propagation of the monsoon ISO? We perform an experiment assuming that the monsoon ISO is nothing but a fluctuation of the ITCZ. First, we carried out an experiment to simulate the basic state annual cycle (CTRL run). As we get a reasonable response from the CTRL run, we seek perturbation response during active conditions by providing a perturbation heat source ($+Q$) over the ITCZ with the S70 diabatic heating profile while a heat sink ($-Q$) in the south with S70 profile. The break condition anomalous response is obtained by reversing the position of heat source and sink. The anomalous Hadley circulation during an active condition with enhanced (decreased) ascending motion to the north (south) of the ITCZ indicates that the particular combination of heat source

and sink with appropriate vertical structure of heating would facilitate northward movement of the heat source. Comparison of this anomalous Hadley circulation to what would result if the heat source and sink also has C100 vertical structure clearly shows that it is the stratiform component that facilitates the northward movement.

[23] The seminal role of the stratiform fraction on the northward propagation of the monsoon ISO indicates that the errors in simulating the boreal summer ISO by climate models may be largely due to inability of the models in simulating the observed proportion of stratiform and convective precipitation. Therefore, serious effort is required to be initiated to improve the parameterization of convection in these models to simulate the observed partitioning between convective and stratiform rains.

References

Bhaskaran, B., J. M. Murphy, and R. G. Jones (1998), Intraseasonal oscillation in the Indian summer monsoon simulated by global and nested regional climate models, *Mon. Weather Rev.*, 126, 3124–3134, doi:10.1175/1520-0493(1998)126<3124:IOITIS>2.0.CO;2.

Chattopadhyay, R., A. K. Sahai, and B. N. Goswami (2008), Objective identification of nonlinear convectively coupled phases of monsoon intraseasonal oscillation: Implications for prediction, *J. Atmos. Sci.*, 65, 1549–1569, doi:10.1175/2007JAS2474.1.

Chen, S. S., R. A. Houze Jr., B. E. Mapes, S. R. Brodzik, and S. E. Yuter (1995), TOGA COARE satellite data summaries available on the World Wide Web, *Bull. Am. Meteorol. Soc.*, 76, 329–333, doi:10.1175/1520-0477(1995)076<0329:TCSDSA>2.0.CO;2.

DeMaria, M. (1985), Linear response of a stratified tropical atmosphere to convective forcing, *J. Atmos. Sci.*, 42, 1944–1959, doi:10.1175/1520-0469(1985)042<1944:LROAST>2.0.CO;2.

Drbohlav, H. K. L., and B. Wang (2007), Horizontal and vertical structures of the northward-propagating intraseasonal oscillation in the south Asian monsoon region simulated by an intermediate model, *J. Clim.*, 20, 4278–4286, doi:10.1175/JCLI4244.1.

Fraedrich, K., E. Kirk, U. Luksch, and F. Lunkeit (2005a), The Portable University Model of the Atmosphere (PUMA): Storm track dynamics and low frequency variability, *Meteorol. Z.*, 14, 735–745, doi:10.1127/0941-2948/2005/0074.

Fraedrich, K., H. Jansen, E. Kirk, and F. Lunkeit (2005b), The Planet Simulator: Green planet and desert world, *Meteorol. Z.*, 14, 305–314, doi:10.1127/0941-2948/2005/0044.

Fu, X., B. Wang, T. Li, and J. P. McCreary (2003), Coupling between northward-propagating, intraseasonal oscillations and sea surface temperature in the Indian Ocean, *J. Atmos. Sci.*, 60, 1733–1753, doi:10.1175/1520-0469(2003)060<1733:CBNIOA>2.0.CO;2.

Gadgil, S., and J. Srinivasan (1990), Low frequency variation of tropical convergence zones, *Meteorol. Atmos. Phys.*, 44, 119–132, doi:10.1007/BF01026814.

Goswami, B. N. (1994), Dynamical predictability of seasonal mean monsoon rainfall: Problems and prospects, *Proc. Indian Natl. Sci. Acad., Part A*, 60, 101–120.

Goswami, B. N. (2005), Intraseasonal variability (ISV) of south Asian summer monsoon, in *Intraseasonal Variability of the Atmosphere-Ocean Climate System*, edited by W. K.-M. Lau and D. E. Waliser, pp. 19–61, Springer, Berlin.

Goswami, B. N., and R. S. Ajaya Mohan (2001), Intraseasonal oscillations and interannual variability of the Indian summer monsoon, *J. Clim.*, 14, 1180–1198, doi:10.1175/1520-0442(2001)014<1180:IOAIVO>2.0.CO;2.

Goswami, B. N., and J. Shukla (1984), Quasi-periodic oscillations in a symmetric general circulation model, *J. Atmos. Sci.*, 41, 20–37, doi:10.1175/1520-0469(1984)041<0020:QPOIAS>2.0.CO;2.

Goswami, B. N., R. S. Ajaya Mohan, P. K. Xavier, and D. Sengupta (2003), Clustering of synoptic activity by Indian summer monsoon intraseasonal oscillations, *Geophys. Res. Lett.*, 30(8), 1431, doi:10.1029/2002GL016734.

Haddad, Z. S., E. A. Smith, C. D. Kummerow, T. Iguchi, M. R. Farrar, S. L. Durden, M. Alves, and W. S. Olson (1997a), The TRMM 'day-1' radar/radiometer combined rain-profiling algorithm, *J. Meteorol. Soc. Jpn.*, 75, 799–809.

Haddad, Z. S., D. A. Short, S. L. Durden, E. Im, S. Hensley, M. B. Grable, and R. A. Black (1997b), A new parametrization of the rain drop size distribution, *IEEE Trans. Geosci. Remote Sens.*, 35, 532–539, doi:10.1109/36.581961.

Hartmann, D. L., H. H. Hendon, and R. A. Houze (1984), Some implications of the mesoscale circulations in tropical cloud clusters for large-scale dynamics and climate, *J. Atmos. Sci.*, 41, 113–121, doi:10.1175/1520-0469(1984)041<0113:SIOTMC>2.0.CO;2.

Houze, R. A., Jr. (1982), Cloud clusters and large-scale vertical motions in the tropics, *J. Meteorol. Soc. Jpn.*, 60, 396–410.

Houze, R. A., Jr. (1988), Convective and stratiform precipitation in the tropics, in *Tropical Rainfall Measurements*, edited by J. S. Theon and N. Fugono, pp. 27–35, A. Deepak, Hampton, Va.

Houze, R. A., Jr. (1989), Observed structure of mesoscale convective systems and implications for large-scale heating, *Q. J. R. Meteorol. Soc.*, 115, 425–461, doi:10.1002/qj.49711548702.

Houze, R. A., Jr. (1997), Stratiform precipitation in regions of convection: A meteorological paradox?, *Bull. Am. Meteorol. Soc.*, 78, 2179–2196, doi:10.1175/1520-0477(1997)078<2179:SPIROC>2.0.CO;2.

Houze, R. A., Jr., D. C. Wilton, and B. F. Smull (2007), Monsoon convection in the Himalayan region as seen by the TRMM precipitation radar, *Q. J. R. Meteorol. Soc.*, 133, 1389–1411.

Hsu, H.-H., C.-H. Weng, and C.-H. Wu (2004), Contrasting characteristics between the northward and eastward propagation of the intraseasonal oscillation during the boreal summer, *J. Clim.*, 17, 727–743, doi:10.1175/1520-0442(2004)017<0727:CCBTNA>2.0.CO;2.

Huffman, G. J., R. F. Adler, M. Morrissey, D. T. Bolvin, S. Curtis, R. Joyce, B. McGavock, and J. Susskind (2001), Global precipitation at one-degree daily resolution from multi-satellite observations, *J. Hydrometeorol.*, 2, 36–50, doi:10.1175/1525-7541(2001)002<0036:GPAODD>2.0.CO;2.

Iguchi, T., T. Kozu, R. Meneghine, J. Awaka, and K. Okamoto (2000), Rain-profiling algorithm for the TRMM precipitation radar, *J. Appl. Meteorol.*, 39, 2038–2052, doi:10.1175/1520-0450(2001)040<2038:RPAFTT>2.0.CO;2.

Jiang, X., T. Li, and B. Wang (2004), Structures and mechanisms of the northward propagating boreal summer intraseasonal oscillation, *J. Clim.*, 17, 1022–1039, doi:10.1175/1520-0442(2004)017<1022:SAMOTN>2.0.CO;2.

Kemball-Cook, S., and B. Wang (2001), Equatorial waves and air-sea interaction in the boreal summer intraseasonal oscillation, *J. Clim.*, 14, 2923–2942, doi:10.1175/1520-0442(2001)014<2923:EWAASI>2.0.CO;2.

Krishnamurti, T. N., and D. Subrahmanyam (1982), The 30–50 day mode at 850 mb during MONEX, *J. Atmos. Sci.*, 39, 2088–2095, doi:10.1175/1520-0469(1982)039<2088:TDMAMD>2.0.CO;2.

Kummerow, C., et al. (2000), The status of the Tropical Rainfall Measuring Mission (TRMM) after two years in orbit, *J. Appl. Meteorol.*, 39, 1965–1982, doi:10.1175/1520-0450(2001)040<1965:TSOTTR>2.0.CO;2.

Kummerow, C., Y. Hong, W. S. Olson, S. Yang, R. F. Adler, J. McCollum, R. Ferraro, G. Petty, D.-B. Shin, and T. T. Wilheit (2001), The evolution of the Goddard profiling algorithm (GPROF) for rainfall estimation from passive microwave sensors, *J. Appl. Meteorol.*, 40, 1801–1840, doi:10.1175/1520-0450(2001)040<1801:TEOTGP>2.0.CO;2.

Lau, K.-M., and P. H. Chan (1986), Aspects of the 40–50 day oscillation during the northern summer as inferred from outgoing longwave radiation, *Mon. Weather Rev.*, 114, 1354–1367, doi:10.1175/1520-0493(1986)114<1354:AOTDOD>2.0.CO;2.

Lau, K.-M., and L. Peng (1987), Origin of low-frequency (intraseasonal) oscillations in the tropical atmosphere. Part I: Basic theory, *J. Atmos. Sci.*, 44, 950–972, doi:10.1175/1520-0469(1987)044<0950:OOLFOI>2.0.CO;2.

Lawrence, D. M., and P. J. Webster (2001), Interannual variations of the intraseasonal oscillation in the south Asian summer monsoon region, *J. Clim.*, 14, 2910–2922, doi:10.1175/1520-0442(2001)014<2910:IVOTIO>2.0.CO;2.

Lee, S.-K., C. Wang, and B. E. Mapes (2009), A simple atmospheric model of the local and teleconnection responses to tropical heating anomalies, *J. Clim.*, 22, 272–284, doi:10.1175/2008JCLI2303.1.

Lin, J., B. E. Mapes, M. Zhang, and M. Newman (2004), Stratiform precipitation, vertical heating profiles, and the Madden-Julian Oscillation, *J. Atmos. Sci.*, 61, 296–309, doi:10.1175/1520-0469(2004)061<0296:SPVHPA>2.0.CO;2.

Lin, X., and R. H. Johnson (1996), Heating, moistening, and rainfall over the western Pacific warm pool during TOGA/COARE, *J. Atmos. Sci.*, 53, 3367–3383, doi:10.1175/1520-0469(1996)053<3367:HMAROT>2.0.CO;2.

Malkus, J. S., and H. Riehl (1964), *Cloud Structure and Distributions Over the Tropical Pacific Ocean*, 229 pp., Univ. of Calif. Press, Berkeley.

Mapes, B. E., and R. A. Houze Jr. (1992), Satellite-observed cloud clusters in the TOGA-COARE domain, *TOGA Notes*, 7, 5–8.

Mapes, B. E., and R. A. Houze Jr. (1995), Diabatic divergence profiles in western Pacific mesoscale convective systems, *J. Atmos. Sci.*, 52, 1807–1828, doi:10.1175/1520-0469(1995)052<1807:DDPIWP>2.0.CO;2.

Nakazawa, T., and K. Rajendran (2004), Asian monsoon rainfall characteristics over land by TRMM satellite and surface station data, paper presented at 2nd TRMM International Science Conference, Japan Aerosp. Explor. Agency, Tokyo, 6–10 Sept.

Ogura, Y., and H. R. Cho (1973), Diagnostic determination of cumulus cloud populations from observed large-scale variables, *J. Atmos. Sci.*, 30, 1276–1286, doi:10.1175/1520-0469(1973)030<1276:DDOCCP>2.0.CO;2.

Rajeevan, M., J. Bhate, J. D. Kale, and B. Lal (2006), High resolution daily gridded rainfall data for the Indian region: Analysis of break and active monsoon spells, *Curr. Sci.*, 91, 296–306.

Ramage, C. S. (1971), *Monsoon Meteorology*, 296 pp., Academic, New York.

Riehl, H., and J. S. Malkus (1958), On the heat balance in the equatorial trough zone, *Geophysica*, 6, 503–538.

Riehl, H., and J. Simpson (1979), The heat balance in the equatorial trough zone, revisited, *Contrib. Atmos. Phys.*, 52, 287–304.

Schumacher, C., R. A. Houze, and I. Kraucunas (2004), The tropical dynamical response to latent heating estimates derived from the TRMM precipitation radar, *J. Atmos. Sci.*, 61, 1341–1358, doi:10.1175/1520-0469(2004)061<1341:TTDRTL>2.0.CO;2.

Sikka, D. R., and S. Gadgil (1980), On the maximum cloud zone and the ITCZ over Indian longitudes during the southwest monsoon, *Mon. Weather Rev.*, 108, 1840–1853, doi:10.1175/1520-0493(1980)108<1840:OTMCZA>2.0.CO;2.

Simpson, J., R. F. Adler, and G. R. North (1988), A proposed Tropical Rainfall Measuring Mission (TRMM) satellite, *Bull. Am. Meteorol. Soc.*, 69, 278–295, doi:10.1175/1520-0477(1988)069<0278:APTRMM>2.0.CO;2.

Srinivasan, J., S. Gadgil, and P. Webster (1993), Meridional propagation of large scale monsoon convective zones, *Meteorol. Atmos. Phys.*, 52, 15–35, doi:10.1007/BF01025750.

Stano, G., T. N. Krishnamurti, T. S. V. Vijaya Kumar, and A. Chakraborty (2002), Hydrometeor structure of a composite monsoon depression using the TRMM radar, *Tellus, Ser. A*, 54(4), 370–381, doi:10.1034/j.1600-0870.2002.01330.x.

Stocker, E., J. Kwiatkowski, and O. Kelley (2001), Gridded hourly text products: A TRMM data reduction approach, in *IGARSS '01 IEEE International Geoscience and Remote Sensing Symposium*, pp. 658–660, Inst. of Electr. and Electron. Eng., New York.

Sui, C.-H., and K.-M. Lau (1989), Origin of low-frequency (intraseasonal) oscilliations in the tropical atmosphere. Part II: Structure and propagation of mobile wave-CISK modes and their modification by lower boundary forcings, *J. Atmos. Sci.*, 46, 37–56, doi:10.1175/1520-0469(1989)046<0037:OOLFOI>2.0.CO;2.

Tao, W. K., et al. (2006), Retrieval of latent heating from TRMM measurements, *Bull. Am. Meteorol. Soc.*, 87, 1555–1572, doi:10.1175/BAMS-87-11-1555.

Waliser, D. (2006), Intraseasonal oscillation, in *The Asian Monsoon*, edited by B. Wang, chap. 5, pp. 203–257, Springer, New York.

Wang, B. (2005), Theory, in *Intraseasonal Variability of the Atmosphere-Ocean Climate System*, edited by W. K.-M. Lau and D. E. Waliser, pp. 307–360, Springer, Berlin.

Wang, B., and H. Rui (1990), Synoptic climatology of transient tropical intraseasonal convection anomalies: 1975–1985, *Meteorol. Atmos. Phys.*, 44, 43–61, doi:10.1007/BF01026810.

Webster, P. J. (1983), Mechanisms of monsoon transition: Surface hydrology effects, *Atmos. Sci.*, 40, 2110–2124, doi:10.1175/1520-0469(1983)040<2110:MOMLFV>2.0.CO;2.

Webster, P. J., V. O. Magaña, T. N. Palmer, J. Shukla, R. A. Tomas, M. Yanai, and T. Yasunari (1998), Monsoons: Processes, predictability, and the prospects for prediction, *J. Geophys. Res.*, 103, 14,451–14,510, doi:10.1029/97JC02719.

Yanai, M., S. Esbensen, and J. H. Chu (1973), Determination of bulk properties of tropical cloud clusters from large-scale heat and moisture budgets, *J. Atmos. Sci.*, 30, 611–627, doi:10.1175/1520-0469(1973)030<0611:DOBPOT>2.0.CO;2.

Yasunari, T. (1979), Cloudiness fluctuation associated with the Northern Hemisphere summer monsoon, *J. Meteorol. Soc. Jpn.*, 57, 227–242.

Yasunari, T. (1980), Quasi-stationary appearance of 30–40 day period in the cloudiness fluctuations during summer monsoon over India, *J. Meteorol. Soc. Jpn.*, 58, 225–229.

_____

R. Chattopadhyay, B. N. Goswami, and A. K. Sahai, Indian Institute of Tropical Meteorology, Pune 411008, India. (rajib@tropmet.res.in)

K. Fraedrich, KlimaCampus, University of Hamburg, Hamburg D-20146, Germany.